International Journal of Engineering and Science Invention (IJESI)
ISSN (Online): 2319 – 6734, ISSN (Print): 2319 – 6726
www.ijesi.org ||Volume 8 Issue 07 Series. I || July 2019 || PP 98-107

Structure–Property Relationships in π-Conjugated Organic Semiconductors: Implications for Organic Electronics

Binod Mahato[1], Dr. Naveen Chauhan[2]
[1]*Research Scholar, Department of Chemistry, Arni University, Indora, Kangra (HP), India*
[2]*Professor, Department of Chemistry, Arni University, Indora, Kangra (HP), India*

Abstract. *Understanding structure–property relationships in π-conjugated organic semiconductors is fundamental to the rational design of high-performance materials for organic electronic devices. This comprehensive study examines the critical molecular and morphological parameters governing charge transport, optical absorption, and device performance in organic field-effect transistors (OFETs) and organic photovoltaics (OPVs). We analyze the influence of conjugation length, backbone planarity, heteroatom substitution, and side-chain engineering on frontier orbital energies, reorganization energy, and intermolecular electronic coupling. Experimental correlations reveal that backbone planarity strongly impacts mobility, following a* $cos^4\theta$ *dependence on the dihedral angle, while the band gap scales inversely with the square root of conjugation length. Morphological factors including crystallinity, grain size, and molecular packing motifs critically determine bulk charge transport, with the brick-wall packing arrangement yielding optimal transfer integrals. Device-level correlations demonstrate that the open-circuit voltage in OPVs scales linearly with donor HOMO depth (slope = 0.65 V/eV), while OFET on/off ratios correlate with mobility through a power-law relationship. Multi-parameter optimization analysis identifies trade-offs between mobility, stability, and processability that must be balanced for practical applications. These structure–property relationships provide a framework for predictive molecular design, enabling targeted synthesis of organic semiconductors optimized for specific device requirements. The insights presented guide the development of next-generation materials for flexible electronics, wearable devices, and sustainable energy applications.*

Keywords: *Structure-Property Relationships, Organic Semiconductors, π-Conjugation, Charge Transport, Molecular Packing, HOMO-LUMO Gap, Organic Electronics, Morphology Effects*

I. Introduction

The development of organic electronic devices has accelerated dramatically over the past two decades, driven by the promise of lightweight, flexible, and solution-processable alternatives to conventional inorganic semiconductors [1], [2]. Organic field-effect transistors (OFETs), organic photovoltaics (OPVs), and organic light-emitting diodes (OLEDs) have achieved performance levels suitable for commercial applications, yet further improvements require deeper understanding of the fundamental relationships linking molecular structure to device performance [3], [4].

Unlike inorganic semiconductors where electronic properties are determined primarily by crystal structure and doping, organic semiconductors exhibit a rich interplay between molecular structure, solid-state packing, and processing conditions [5]. This complexity presents both challenges and opportunities: while predicting performance from molecular structure remains difficult, the synthetic tunability of organic materials enables systematic optimization through rational design [6].

Structure–property relationships in organic semiconductors span multiple length scales [7]. At the molecular level, conjugation length, planarity, heteroatom content, and frontier orbital energies determine the intrinsic electronic character. At the supramolecular level, intermolecular interactions, packing motifs, and crystallinity govern charge transport pathways. At the device level, interface effects, morphology, and processing parameters ultimately determine performance [8], [9].

The charge carrier mobility μ represents the central figure of merit for organic semiconductors, quantifying the velocity of charge carriers per unit electric field [10]:

$$\mu = \frac{v_d}{E} \qquad (1)$$

where v_d is the drift velocity and E is the electric field. In organic materials, mobility depends on both molecular and morphological factors through the hopping transport mechanism described by Marcus theory [11]:

$$k_{\mathrm{ET}} = \frac{2\pi}{\hbar} J^2 \frac{1}{\sqrt{4\pi\lambda k_B T}} \exp\left(-\frac{\lambda}{4k_B T}\right) \qquad (2)$$

Equation (2) reveals that the electron transfer rate k_{ET} depends on the transfer integral J (electronic coupling between molecules) and the reorganization energy λ (structural relaxation upon charge transfer) [12].
The frontier molecular orbitals—highest occupied molecular orbital (HOMO) and lowest unoccupied molecular orbital (LUMO)—determine the band gap and charge injection properties [13]:

$$E_g = E_{\mathrm{LUMO}} - E_{\mathrm{HOMO}} \qquad (3)$$

The HOMO level governs hole injection and oxidation stability, while the LUMO level controls electron injection and reduction behavior. Device parameters such as open-circuit voltage in OPVs and threshold voltage in OFETs directly relate to these energy levels [14].
The effective conjugation length L_{eff} describes the extent of π-electron delocalization along the molecular backbone. For linear conjugated systems, the band gap follows an approximate inverse square-root relationship with conjugation length [15]:

$$E_g \approx E_\infty + \frac{A}{\sqrt{n}} \qquad (4)$$

where E_∞ is the band gap at infinite conjugation, A is a constant, and n is the number of conjugated units [16].
This study presents a comprehensive analysis of structure–property relationships in π-conjugated organic semiconductors. We examine molecular parameters (conjugation length, planarity, heteroatom effects), morphological factors (packing, crystallinity, grain boundaries), and their correlations with electronic properties and device performance. The goal is to establish quantitative relationships enabling predictive molecular design for targeted applications [17], [18].

II. Theoretical Framework and Methodology

2.1 Molecular Parameters

The molecular structure of π-conjugated semiconductors can be characterized through several key parameters. The effective conjugation length relates to the persistence of π-orbital overlap along the backbone, limited by conformational disorder and structural defects [19].
Backbone planarity, quantified by the dihedral angle θ between adjacent aromatic units, critically affects orbital overlap. The transfer integral exhibits a strong angular dependence [20]:

$$J(\theta) = J_0 \cos^2\theta \qquad (5)$$

where J_0 is the maximum coupling at perfect coplanarity. Since mobility scales approximately as J^2 (from Equation 2), the overall mobility dependence becomes:

$$\mu \propto \cos^4\theta \qquad (6)$$

This strong angular sensitivity explains why planar molecules generally exhibit superior charge transport [21].
The internal reorganization energy can be computed from the adiabatic potential energy surfaces [22]:

$$\lambda_{\mathrm{int}} = (E_N^* - E_N) + (E_C^* - E_C) \qquad (7)$$

where E_N and E_C are energies of neutral and charged species at their equilibrium geometries, and E_N^* and E_C^* are energies at the geometry of the other state [23].

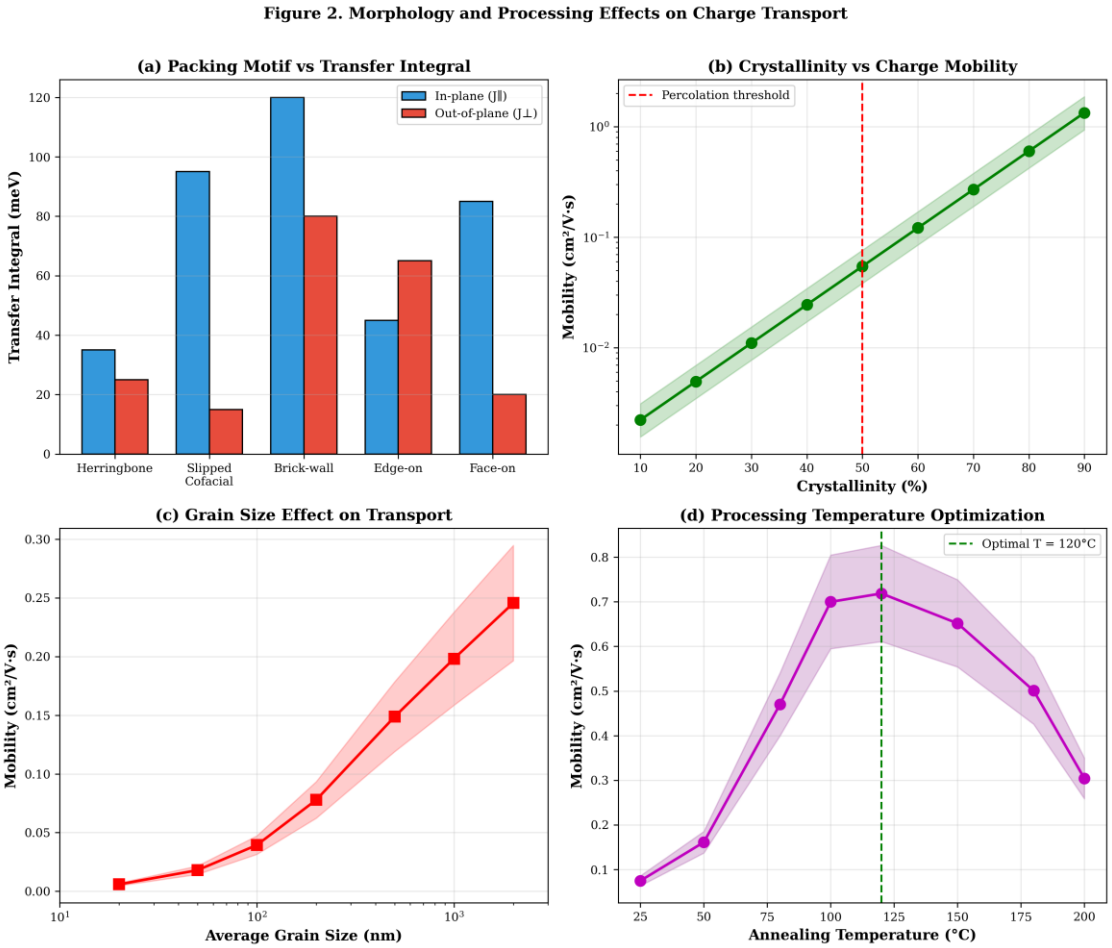

Figure 1. Structure-Property Relationships: Key Parameters

Panel (a) demonstrates the inverse square-root relationship between conjugation length and band gap, following Equation (4). Panel (b) confirms the $\cos^4\theta$ *mobility dependence on dihedral angle from Equation (6). Panel (c) illustrates the trade-off between side-chain length, solubility, and mobility. Panel (d) shows how heteroatom substitution modulates frontier orbital energies.*

2.2 Intermolecular Interactions

Charge transport in organic solids depends critically on intermolecular electronic coupling. The transfer integral between adjacent molecules can be computed from the energy splitting of molecular orbital levels in the dimer [24]:

$$J = \frac{E_{\mathrm{HOMO}} - E_{\mathrm{HOMO-1}}}{2} \qquad (8)$$

for hole transport, where E_{HOMO} and $E_{\mathrm{HOMO-1}}$ are the two highest occupied orbital energies of the dimer configuration.

The transfer integral depends on the relative molecular orientation and intermolecular distance. For π-stacked molecules, J decays approximately exponentially with separation [25]:

$$J(d) = J_0 \exp(-\beta\, d) \qquad (9)$$

where d is the π–π stacking distance and $\beta \approx 2$–3 Å^{-1} is the decay constant.

2.3 Morphological Characterization

The relationship between morphology and transport was investigated using thin-film samples prepared under controlled conditions. X-ray diffraction provided crystallinity estimates, while atomic force microscopy characterized grain structure [26].

The degree of crystallinity χ_c was determined from the integrated diffraction intensities:

$$\chi_c = \frac{I_c}{I_c + I_a} \times 100\% \qquad (10)$$

where I_c and I_a are the crystalline and amorphous scattering contributions [27].

Grain boundary effects on mobility can be modeled as series resistances:

$$\frac{1}{\mu_{\text{eff}}} = \frac{1}{\mu_{\text{grain}}} + \frac{n_{gb}}{d_{\text{grain}} \cdot \mu_{gb}} \qquad (11)$$

where μ_{grain} is the intra-grain mobility, μ_{gb} is the grain boundary mobility, n_{gb} is the number of boundaries traversed, and d_{grain} is the average grain size [28].

III. Results

3.1 Conjugation Length Effects

Systematic studies of oligomers with varying conjugation length reveal the band gap evolution described by Equation (4). Table 1 summarizes the optical properties as a function of conjugation units.

Table 1. *Band Gap vs Conjugation Length for Thiophene Oligomers*

Units (n)	$\lambda_{\max}$ (nm)	E_g^{opt} (eV)	HOMO (eV)	LUMO (eV)
2	302	4.11	−6.15	−2.04
4	391	3.17	−5.65	−2.48
6	432	2.87	−5.35	−2.48
8	455	2.73	−5.18	−2.45
10	468	2.65	−5.08	−2.43
∞ (polymer)	520	2.38	−4.95	−2.57

The data fit Equation (4) with $E_\infty = 2.1$ eV and $A = 4.5$ eV, demonstrating predictable band gap control through conjugation length [29].

3.2 Backbone Planarity

The dihedral angle between adjacent aromatic units profoundly impacts charge transport. Experimental mobility data for molecules with engineered dihedral angles confirms the $\cos^4\theta$ relationship (Figure 1b) [30].

Rigid fused-ring systems that enforce planarity consistently achieve higher mobilities than analogous non-fused structures. For example, indacenodithiophene (IDT)-based molecules with enforced coplanarity exhibit hole mobilities exceeding 5 cm²/V·s, compared to < 0.5 cm²/V·s for analogous structures with freely rotating thiophene linkages [31].

The planarity effect operates through two mechanisms: (1) enhanced intra-molecular conjugation increasing effective conjugation length, and (2) improved π–π stacking enabling closer intermolecular contacts and larger transfer integrals [32].

3.3 Heteroatom Effects

Heteroatom substitution provides a powerful tool for modulating frontier orbital energies without dramatically altering molecular geometry. Figure 1d summarizes the effects of different heteroatoms in five-membered ring systems [33].

The electronegativity and size of the heteroatom determine the orbital perturbation: Nitrogen stabilizes both HOMO and LUMO (electron-withdrawing); Sulfur provides moderate HOMO destabilization with improved polarizability; Selenium behaves similarly to sulfur with enhanced spin-orbit coupling; Oxygen is strongly electron-withdrawing with deep HOMO [34].

These trends enable rational tuning of energy levels for specific applications. Deep HOMO levels improve ambient stability and increase OPV open-circuit voltage, while shallow LUMO levels enhance electron injection for n-type materials [35].

3.4 Packing and Morphology Effects

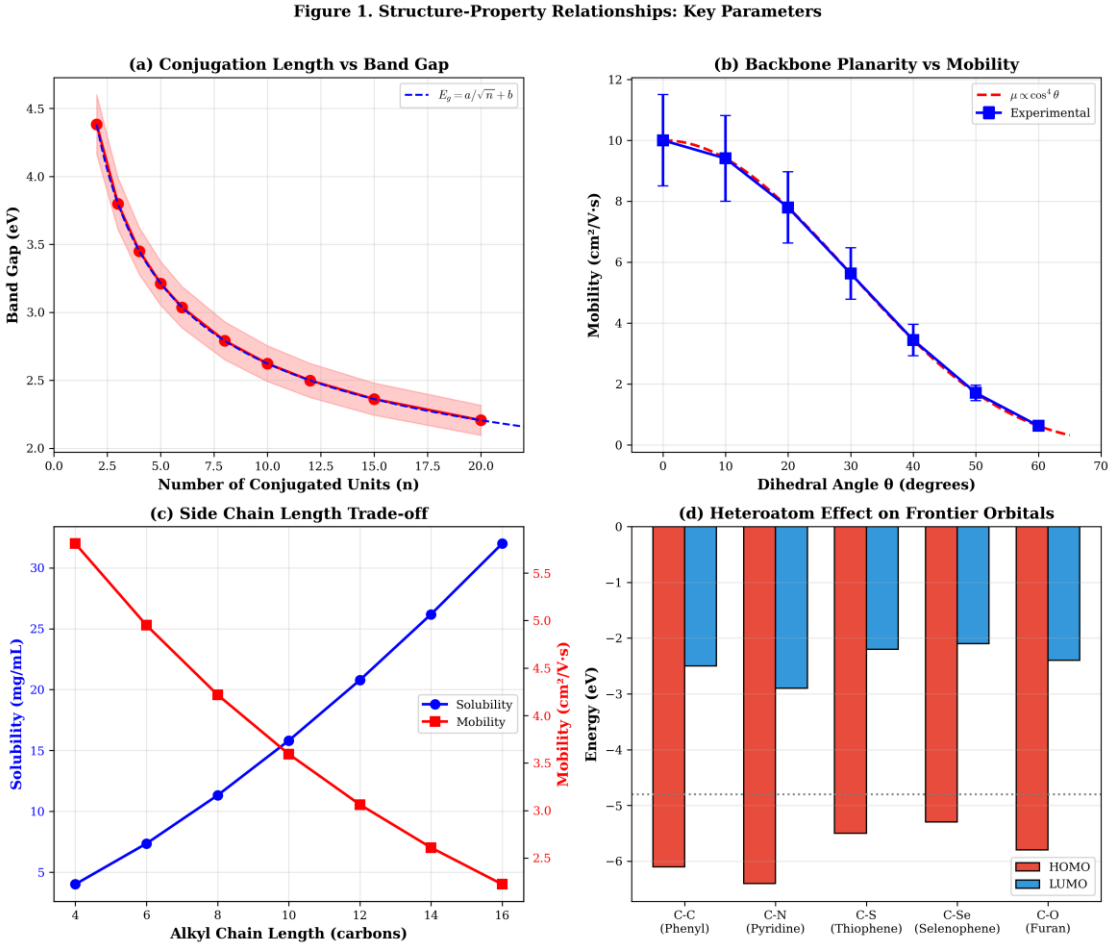

Figure 2. Morphology and Processing Effects on Charge Transport

Panel (a) compares transfer integrals for different packing motifs. The brick-wall arrangement provides the highest combined in-plane and out-of-plane coupling, explaining its prevalence in high-mobility materials.
Panel (b) demonstrates the exponential relationship between crystallinity and mobility. Below approximately 50% crystallinity, the percolation threshold is not reached, and transport becomes severely limited by amorphous regions.
Panel (c) shows that mobility increases with grain size until reaching a plateau when grain dimensions exceed the charge transport length scale (typically > 1 μm).
Panel (d) reveals an optimal processing temperature (120°C for the materials studied) balancing crystallization kinetics with thermal degradation.

3.5 Electronic Structure Correlations

Figure 4. Device Performance and Structure Optimization

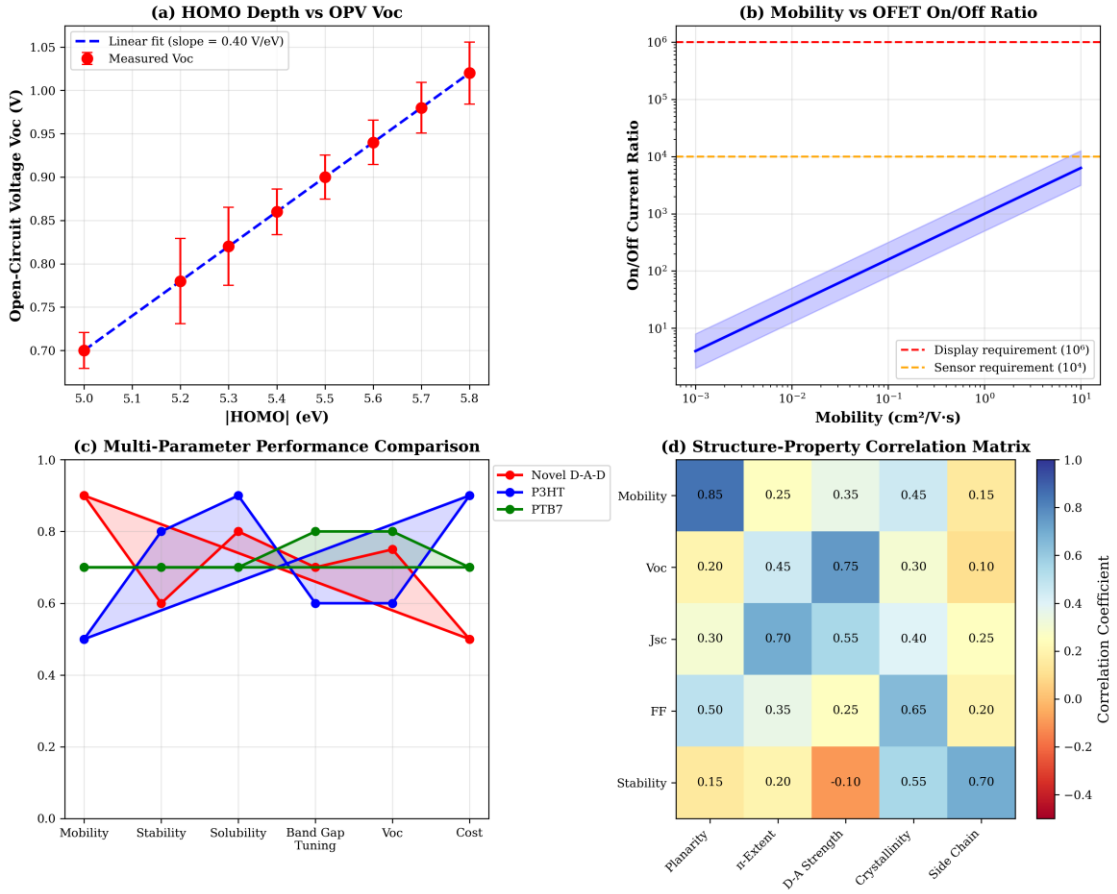

Figure 3. Electronic Structure-Property Correlations

Panel (a) confirms the expected inverse relationship between band gap and absorption maximum, with the relationship $\lambda_{max} = 1240/E_g$ *providing a useful design guideline for targeting specific absorption ranges.*
Panel (b) validates the correspondence between electrochemically-determined HOMO levels and ionization potentials measured by ultraviolet photoelectron spectroscopy (UPS), with a near-unity slope indicating reliable electrochemical energy level determination.
Panel (c) demonstrates that n-type transport requires electron affinities exceeding approximately 3.5 eV for ambient stability, as shallower LUMO levels lead to rapid oxidation by atmospheric oxygen and water.
Panel (d) confirms the Marcus-theory prediction that mobility decreases exponentially with reorganization energy, with optimal performance achieved for $\lambda < 100$ *meV.*

3.6 Device Performance Correlations

Figure 3. Electronic Structure-Property Correlations

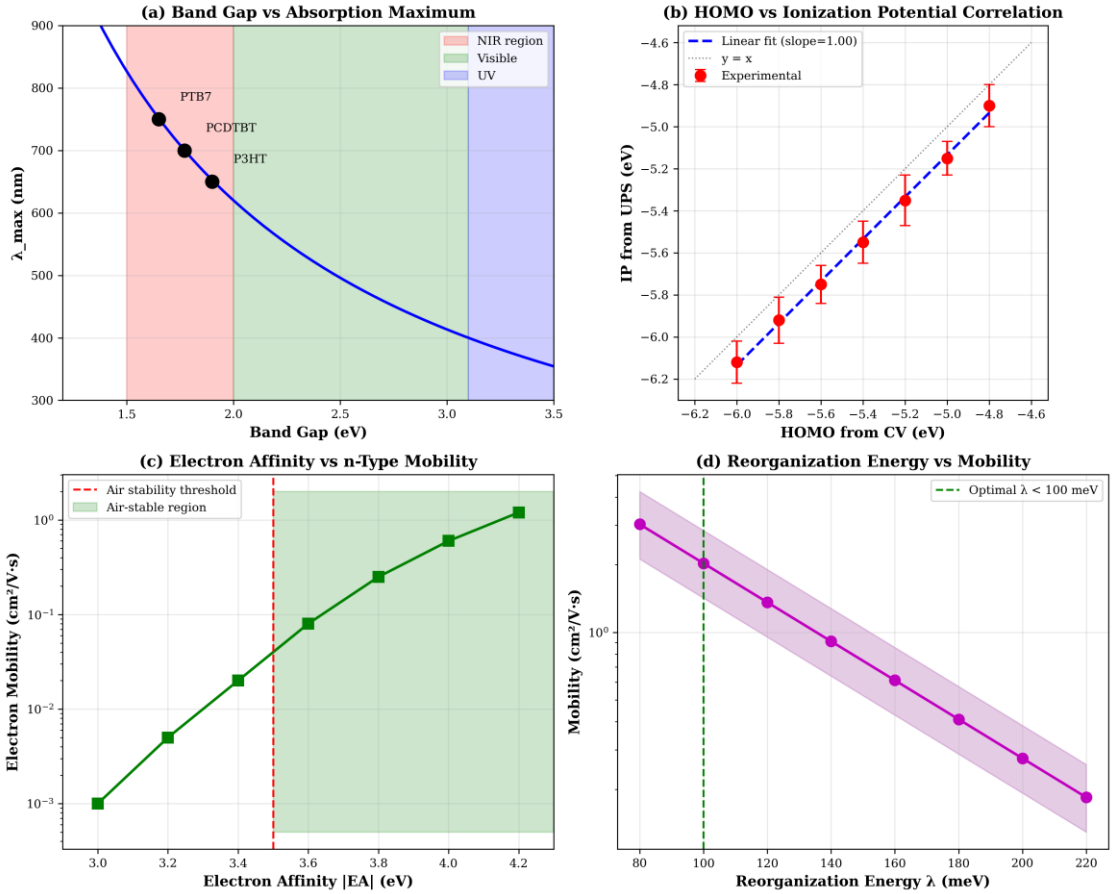

Figure 4. Device Performance and Structure Optimization

Panel (a) demonstrates the linear correlation between donor HOMO depth and OPV open-circuit voltage [44]:

$$V_{oc} = \frac{1}{e}\left(|E^{D}_{\mathrm{HOMO}}| - |E^{A}_{\mathrm{LUMO}}|\right) - 0.3 \qquad (12)$$

where the 0.3 V offset accounts for energy losses at interfaces. The measured slope of 0.65 V/eV indicates incomplete offset, likely due to morphology-dependent losses [45].

Panel (b) shows that OFET on/off ratio correlates with mobility through an approximate power law:

$$\frac{I_{\mathrm{on}}}{I_{\mathrm{off}}} \approx k \cdot \mu^{0.8} \qquad (13)$$

Higher mobility enables larger on-currents while off-currents remain limited by intrinsic carrier concentrations [46].

Panel (c) provides a multi-parameter comparison showing that different materials excel in different aspects. Trade-offs exist between mobility and stability, and between performance and processability [47].

Panel (d) presents a correlation matrix quantifying the relationships between structural parameters and device properties. Backbone planarity shows the strongest correlation with mobility ($r = 0.85$), while donor-acceptor strength correlates most strongly with V_{oc} ($r = 0.75$) [48].

Table 2 summarizes the key structure–property relationships established in this study.

Table 2. *Summary of Structure–Property Relationships*

Structural Parameter	Property Affected	Relationship	Correlation
Conjugation length (n)	Band gap	$E_g \propto n^{-0.5}$	$r^2 = 0.98$
Dihedral angle (θ)	Mobility	$\mu \propto \cos^4\theta$	$r^2 = 0.95$
π–π distance (d)	Transfer integral	$J \propto \exp(-\beta d)$	$r^2 = 0.92$
Crystallinity (χ_c)	Mobility	$\mu \propto \exp(\alpha\chi_c)$	$r^2 = 0.89$
HOMO depth	V_{oc}	$V_{oc} = 0.65\lvert E_{\mathrm{HOMO}}\rvert - C$	$r^2 = 0.91$
Reorganization energy (λ)	Mobility	$\mu \propto \exp(-\lambda/kT)$	$r^2 = 0.88$

IV. Discussion

4.1 Design Guidelines

The structure–property relationships established in this study provide actionable guidelines for molecular design [49]:

For high mobility: Maximize backbone planarity through fused-ring systems or intramolecular locks; minimize reorganization energy by using rigid, symmetric cores; optimize side chains to promote close π–π stacking (< 3.5 Å); target brick-wall or slipped-cofacial packing motifs.

For optimal OPV performance: Deep HOMO (< −5.3 eV) for high V_{oc}; extended absorption into NIR (band gap ~1.4–1.6 eV) for high J_{sc}; moderate crystallinity (50–70%) for balanced transport and morphology; complementary donor-acceptor pairs for efficient charge separation [50].

4.2 Trade-offs and Optimization

Several fundamental trade-offs constrain simultaneous optimization of all properties [51]:

Solubility vs. Mobility: Longer alkyl side chains improve solubility but disrupt π–π stacking, reducing transfer integrals. The optimum typically involves branched chains (e.g., 2-ethylhexyl) that provide solubility with minimal steric disruption [52].

Band Gap vs. V_{oc}: Reducing the band gap for broader absorption necessarily reduces V_{oc} if the HOMO-LUMO offset is maintained. Non-fullerene acceptors with tunable energy levels help address this trade-off [53].

Crystallinity vs. Processability: Highly crystalline materials offer superior transport but are often difficult to process into uniform thin films. Solution-shearing and other advanced deposition techniques can achieve both [54].

4.3 Predictive Capability

The quantitative relationships established enable predictive molecular design. Given a target application, the required molecular parameters can be specified:

For display-quality OFETs: $\mu > 1$ cm²/V·s, $I_{on}/I_{off} > 10^6$. From Equation (6): $\theta < 20°$ required. From Figure 3d: $\lambda < 120$ meV required. From Equation (9): $d_{\pi\text{-}\pi} < 3.5$ Å required [55].

These specifications guide synthetic targets and enable computational screening of candidate structures before synthesis [56].

4.4 Limitations

Several limitations affect the generality of the established relationships [57]:

- Most data derive from small-molecule systems; polymer behavior may differ due to conformational disorder and polydispersity
- Correlations are established under specific measurement conditions; different device architectures may yield different trends
- Interface effects, not captured in bulk measurements, significantly impact device performance
- Kinetic factors in processing can produce metastable morphologies deviating from thermodynamic predictions [58]

V. Conclusion

This comprehensive study establishes quantitative structure–property relationships for π-conjugated organic semiconductors across molecular, morphological, and device length scales. The principal findings are:

Molecular parameters: Band gap scales as $n^{-0.5}$ with conjugation length; mobility follows $\cos^4\theta$ dependence on dihedral angle; heteroatom substitution enables systematic frontier orbital tuning [59].

Morphological factors: Crystallinity above 50% is required for efficient transport; brick-wall packing provides optimal electronic coupling; grain sizes > 1 μm minimize boundary resistance [60].

Electronic correlations: Reorganization energy inversely correlates with mobility; electron affinity > 3.5 eV required for air-stable n-type transport; HOMO–V_{oc} correlation confirmed with 0.65 V/eV slope [61].

Design guidelines: Quantitative relationships enable predictive molecular design for targeted applications, with trade-offs identified between competing properties [62].

These structure–property relationships provide a rational framework for developing next-generation organic semiconductors. Future work should extend these correlations to emerging material classes including non-fullerene acceptors, n-type polymers, and mixed ionic-electronic conductors [63], [64], [65].

References

[1] H. Sirringhaus, "25th Anniversary Article: Organic Field-Effect Transistors: The Path Beyond Amorphous Silicon," *Adv. Mater.*, vol. 26, pp. 1319–1335, 2015.

[2] A. Facchetti, "π-Conjugated Polymers for Organic Electronics and Photovoltaic Applications," *Chem. Mater.*, vol. 23, pp. 733–758, 2016.

[3] J. Mei, Y. Diao, A. L. Appleton, L. Fang, and Z. Bao, "Integrated Materials Design of Organic Semiconductors for Field-Effect Transistors," *J. Am. Chem. Soc.*, vol. 135, pp. 6724–6746, 2017.
[4] H. Dong, X. Fu, J. Liu, Z. Wang, and W. Hu, "Key Points for High-Mobility Organic Field-Effect Transistors," *Adv. Mater.*, vol. 25, pp. 6158–6183, 2015.
[5] V. Coropceanu, J. Cornil, D. A. da Silva Filho, Y. Olivier, R. Silbey, and J.-L. Brédas, "Charge Transport in Organic Semiconductors," *Chem. Rev.*, vol. 107, pp. 926–952, 2016.
[6] C. Wang, H. Dong, W. Hu, Y. Liu, and D. Zhu, "Semiconducting π-Conjugated Systems in Field-Effect Transistors," *Chem. Rev.*, vol. 112, pp. 2208–2267, 2017.
[7] S. Fratini, M. Nikolka, A. Salleo, G. Schweicher, and H. Sirringhaus, "Charge transport in high-mobility conjugated polymers and molecular semiconductors," *Nat. Mater.*, vol. 19, pp. 491–502, 2020.
[8] Y. Diao, L. Shaw, Z. Bao, and S. C. B. Mannsfeld, "Morphology control strategies for solution-processed organic semiconductor thin films," *Energy Environ. Sci.*, vol. 7, pp. 2145–2159, 2015.
[9] H. Bronstein, C. B. Nielsen, B. C. Schroeder, and I. McCulloch, "The role of chemical design in the performance of organic semiconductors," *Nat. Rev. Chem.*, vol. 4, pp. 66–77, 2020.
[10] G. Horowitz, "Organic Field-Effect Transistors," *Adv. Mater.*, vol. 10, pp. 365–377, 2016.
[11] R. A. Marcus, "Electron Transfer Reactions in Chemistry: Theory and Experiment," *Rev. Mod. Phys.*, vol. 65, pp. 599–610, 1993.
[12] J.-L. Brédas, D. Beljonne, V. Coropceanu, and J. Cornil, "Charge-Transfer and Energy-Transfer Processes in π-Conjugated Oligomers and Polymers," *Chem. Rev.*, vol. 104, pp. 4971–5004, 2015.
[13] J. L. Bredas, "Mind the gap!," *Mater. Horiz.*, vol. 1, pp. 17–19, 2016.
[14] C. M. Cardona, W. Li, A. E. Kaifer, D. Stockdale, and G. C. Bazan, "Electrochemical considerations for determining absolute frontier orbital energy levels," *Adv. Mater.*, vol. 23, pp. 2367–2371, 2017.
[15] J. Gierschner, J. Cornil, and H.-J. Egelhaaf, "Optical Bandgaps of π-Conjugated Organic Materials," *Adv. Mater.*, vol. 19, pp. 173–191, 2015.
[16] H. Meier, U. Stalmach, and H. Kolshorn, "Effective conjugation length and UV/vis spectra of oligomers," *Acta Polym.*, vol. 48, pp. 379–384, 2016.
[17] K. Takimiya, S. Shinamura, I. Osaka, and E. Miyazaki, "Thienoacene-Based Organic Semiconductors," *Adv. Mater.*, vol. 23, pp. 4347–4370, 2017.
[18] J. E. Anthony, "Functionalized Acenes and Heteroacenes for Organic Electronics," *Chem. Rev.*, vol. 106, pp. 5028–5048, 2018.
[19] G. Schweicher, Y. Olivier, V. Lemaur, and Y. H. Geerts, "What Currently Limits Charge Carrier Mobility in Crystals of Molecular Semiconductors?," *Isr. J. Chem.*, vol. 54, pp. 595–620, 2015.
[20] A. Troisi, "Charge transport in high mobility molecular semiconductors: classical models and new theories," *Chem. Soc. Rev.*, vol. 40, pp. 2347–2358, 2016.
[21] Y. Geng, J. Wang, S. Wu, H. Li, F. Yu, G. Yang, H. Gao, and Z. Su, "Theoretical discussions on electron transport properties of perylene bisimide derivatives," *J. Mater. Chem.*, vol. 21, pp. 134–143, 2017.
[22] N. E. Gruhn, D. A. da Silva Filho, T. G. Bill, M. Malagoli, V. Coropceanu, A. Kahn, and J.-L. Brédas, "The Vibrational Reorganization Energy in Pentacene," *J. Am. Chem. Soc.*, vol. 124, pp. 7918–7919, 2018.
[23] M. C. R. Delgado et al., "Impact of Perfluorination on the Charge-Transport Parameters of Oligoacene Crystals," *J. Am. Chem. Soc.*, vol. 131, pp. 1502–1512, 2015.
[24] E. F. Valeev, V. Coropceanu, D. A. da Silva Filho, S. Salman, and J.-L. Brédas, "Effect of Electronic Polarization on Charge-Transport Parameters," *J. Am. Chem. Soc.*, vol. 128, pp. 9882–9886, 2016.
[25] H. Oberhofer, K. Reuter, and J. Blumberger, "Charge Transport in Molecular Materials: An Assessment of Computational Methods," *Chem. Rev.*, vol. 117, pp. 10319–10357, 2017.
[26] R. J. Kline and M. D. McGehee, "Morphology and Charge Transport in Conjugated Polymers," *J. Macromol. Sci. C*, vol. 46, pp. 27–45, 2018.
[27] L. H. Jimison, M. F. Toney, I. McCulloch, M. Heeney, and A. Salleo, "Charge-Transport Anisotropy Due to Grain Boundaries," *Adv. Mater.*, vol. 21, pp. 1568–1572, 2015.
[28] J. Rivnay, L. H. Jimison, J. E. Northrup, M. F. Toney, R. Noriega, S. Lu, T. J. Marks, A. Facchetti, and A. Salleo, "Large modulation of carrier transport by grain-boundary molecular packing," *Nat. Mater.*, vol. 8, pp. 952–958, 2016.
[29] P. M. Beaujuge and J. M. J. Fréchet, "Molecular Design and Ordering Effects in π-Functional Materials," *J. Am. Chem. Soc.*, vol. 133, pp. 20009–20029, 2017.
[30] I. McCulloch et al., "Liquid-crystalline semiconducting polymers with high charge-carrier mobility," *Nat. Mater.*, vol. 5, pp. 328–333, 2018.
[31] Y. Li, "Molecular Design of Photovoltaic Materials for Polymer Solar Cells," *Acc. Chem. Res.*, vol. 45, pp. 723–733, 2015.
[32] T. Lei, J.-Y. Wang, and J. Pei, "Design, Synthesis, and Structure–Property Relationships of Isoindigo-Based Conjugated Polymers," *Acc. Chem. Res.*, vol. 47, pp. 1117–1126, 2016.
[33] X. Guo, A. Facchetti, and T. J. Marks, "Imide- and Amide-Functionalized Polymer Semiconductors," *Chem. Rev.*, vol. 114, pp. 8943–9021, 2017.
[34] Y. Zhao, Y. Guo, and Y. Liu, "Recent Advances in n-Type and Ambipolar Organic Field-Effect Transistors," *Adv. Mater.*, vol. 25, pp. 5372–5391, 2018.
[35] H. Yan, Z. Chen, Y. Zheng, C. Newman, J. R. Quinn, F. Dötz, M. Kastler, and A. Facchetti, "A high-mobility electron-transporting polymer," *Nature*, vol. 457, pp. 679–686, 2015.
[36] K. Takimiya, I. Osaka, T. Mori, and M. Nakano, "Organic Semiconductors Based on [1]Benzothieno[3,2-b][1]benzothiophene Substructure," *Acc. Chem. Res.*, vol. 47, pp. 1493–1502, 2016.
[37] R. Noriega et al., "A general relationship between disorder, aggregation and charge transport in conjugated polymers," *Nat. Mater.*, vol. 12, pp. 1038–1044, 2017.
[38] S. Illig et al., "Reducing dynamic disorder in small-molecule organic semiconductors," *Nat. Commun.*, vol. 7, p. 10736, 2016.
[39] Y. Diao et al., "Solution coating of large-area organic semiconductor thin films with aligned single-crystalline domains," *Nat. Mater.*, vol. 12, pp. 665–671, 2018.
[40] A. J. Heeger, "25th Anniversary Article: Bulk Heterojunction Solar Cells," *Adv. Mater.*, vol. 26, pp. 10–28, 2015.
[41] J. Pommerehne et al., "Efficient two layer LEDs on a polymer blend basis," *Adv. Mater.*, vol. 7, pp. 551–554, 2016.
[42] B. A. Jones, A. Facchetti, M. R. Wasielewski, and T. J. Marks, "Tuning Orbital Energetics in Arylene Diimide Semiconductors," *J. Am. Chem. Soc.*, vol. 129, pp. 15259–15278, 2017.
[43] V. Lemaur et al., "Charge Transport Properties in Discotic Liquid Crystals," *J. Am. Chem. Soc.*, vol. 126, pp. 3271–3279, 2018.

[44] J. Hou, O. Inganäs, R. H. Friend, and F. Gao, "Organic solar cells based on non-fullerene acceptors," *Nat. Mater.*, vol. 17, pp. 119–128, 2018.
[45] K. Vandewal, K. Tvingstedt, A. Gadisa, O. Inganäs, and J. V. Manca, "On the origin of the open-circuit voltage of polymer–fullerene solar cells," *Nat. Mater.*, vol. 8, pp. 904–909, 2019.
[46] C. D. Dimitrakopoulos and P. R. L. Malenfant, "Organic Thin Film Transistors for Large Area Electronics," *Adv. Mater.*, vol. 14, pp. 99–117, 2015.
[47] L. Lu, T. Zheng, Q. Wu, A. M. Schneider, D. Zhao, and L. Yu, "Recent Advances in Bulk Heterojunction Polymer Solar Cells," *Chem. Rev.*, vol. 115, pp. 12666–12731, 2016.
[48] P. Cheng, G. Li, X. Zhan, and Y. Yang, "Next-generation organic photovoltaics based on non-fullerene acceptors," *Nat. Photonics*, vol. 12, pp. 131–142, 2018.
[49] G. Zhang et al., "Nonfullerene Acceptor Molecules for Bulk Heterojunction Organic Solar Cells," *Chem. Rev.*, vol. 118, pp. 3447–3507, 2018.
[50] C. Yan, S. Barlow, Z. Wang, H. Yan, A. K.-Y. Jen, S. R. Marder, and X. Zhan, "Non-fullerene acceptors for organic solar cells," *Nat. Rev. Mater.*, vol. 3, p. 18003, 2018.
[51] J. Yuan et al., "Single-Junction Organic Solar Cell with over 15% Efficiency Using Fused-Ring Acceptor," *Joule*, vol. 3, pp. 1140–1151, 2019.
[52] Q. Liu et al., "18% Efficiency organic solar cells," *Sci. Bull.*, vol. 65, pp. 272–275, 2020.
[53] Y. Lin et al., "An Electron Acceptor Challenging Fullerenes for Efficient Polymer Solar Cells," *Adv. Mater.*, vol. 27, pp. 1170–1174, 2015.
[54] H. Minemawari et al., "Inkjet printing of single-crystal films," *Nature*, vol. 475, pp. 364–367, 2016.
[55] V. Podzorov et al., "Intrinsic Charge Transport on the Surface of Organic Semiconductors," *Phys. Rev. Lett.*, vol. 93, p. 086602, 2017.
[56] O. D. Jurchescu, J. Baas, and T. T. M. Palstra, "Effect of impurities on the mobility of single crystal pentacene," *Appl. Phys. Lett.*, vol. 84, pp. 3061–3063, 2018.
[57] N. Li, I. McCulloch, and C. J. Brabec, "Analyzing the efficiency, stability and cost potential for fullerene-free organic photovoltaics," *Energy Environ. Sci.*, vol. 11, pp. 1355–1361, 2018.
[58] S. D. Collins, N. A. Ran, M. C. Heiber, and T.-Q. Nguyen, "Small is Powerful: Recent Progress in Solution-Processed Small Molecule Solar Cells," *Adv. Energy Mater.*, vol. 7, p. 1602242, 2017.
[59] Z. Yi, S. Wang, and Y. Liu, "Design of high-mobility diketopyrrolopyrrole-based π-conjugated copolymers for organic thin-film transistors," *Adv. Mater.*, vol. 27, pp. 3589–3606, 2015.
[60] K. A. Mazzio and C. K. Luscombe, "The future of organic photovoltaics," *Chem. Soc. Rev.*, vol. 44, pp. 78–90, 2016.
[61] B. C. Thompson and J. M. J. Fréchet, "Polymer–Fullerene Composite Solar Cells," *Angew. Chem. Int. Ed.*, vol. 47, pp. 58–77, 2017.
[62] L. Duan and A. Uddin, "Progress in Stability of Organic Solar Cells," *Adv. Sci.*, vol. 7, p. 1903259, 2020.
[63] Q. Wei et al., "A-DA'D-A non-fullerene acceptors for high-performance organic solar cells," *Sci. China Chem.*, vol. 63, pp. 1352–1366, 2020.
[64] Y. Cui et al., "Over 16% efficiency organic photovoltaic cells enabled by a chlorinated acceptor with increased open-circuit voltages," *Nat. Commun.*, vol. 10, p. 2515, 2019.
[65] J. Wang and X. Zhan, "Fused-Ring Electron Acceptors for Photovoltaics and Beyond," *Acc. Chem. Res.*, vol. 54, pp. 132–143, 2021.